ORIGINAL PAPER

On a Paradox of Elasto-Plastic Tunnel Analysis

L. Cantieni · G. Anagnostou

Abstract Elasto-plastic tunnel analysis may produce a paradox in the calculation of ground pressure whereby ground pressures appear to increase in relation to higher ground quality. More specifically, for an overstressed ground in combination with a stiff support, analysis may indicate greater loading of the support with a ground of high strength than with a ground of low strength (all of the other parameters being equal). This counter-intuitive outcome appears in all of the common calculation models (analytical plane strain analysis, numerical plane strain analysis and numerical axisymmetric analysis), although it does not correspond either to the ground behaviour that is intuitively expected or to ground behaviour observed in the field, thus raising doubts over the predictive power of common tunnel design calculations. The present paper discusses the assumptions made in the models that are responsible for the paradox: the assumption that ground behaviour is time-independent (whereas in reality over-stressed ground generally creeps) and the assumption that the support operates with full stiffness close to the face (which is not feasible in reality due to the nature of construction procedures). When proper account is taken of either or both of these assumptions in more advanced models, the paradox disappears. As the models which generate the paradox are very commonly used in engineering and scientific practice, the investigations of the present paper may be of value, helping the engineer to understand the uncertainties inherent in the models and to arrive at a better interpretation of the results they produce.

List of symbols

a	Tunnel radius
d	Lining thickness
d_S	Thickness of the TBM shield
E	Young's modulus of the ground
E_L	Young's modulus of the lining
$E_{L,28}$	Young's modulus of the lining after 28 days ($=E_L$)
E_S	Young's modulus of the TBM shield
$E_L(t)$	Time-dependent Young's modulus of the lining
e	Unsupported span
f	Yield function
f_c	Uniaxial compressive strength of the ground
g	Plastic potential
i	Point/interval (defined in Fig. 22)
j	Point/interval (defined in Fig. 22)
k	Lining stiffness
k_I	Support stiffness before the deformation phase of the yielding support
k_j	Average stiffness over the integration interval j
$k^{(i)}$	Stiffness of the fictitious lining layer i
k_S	Stiffness of the TBM Shield
m	Point/interval (defined in Fig. 22)
M	Bending moment
N	Hoop force
p	Rock pressure acting upon the lining
p_F	Face support pressure
p_I	Fictitious internal pressure in the plane strain analysis
p_j	Rock pressure at the point j
$p_j^{(i)}$	Pressure exerted by layer i at point j
p_y	Yielding support pressure

L. Cantieni (✉) · G. Anagnostou
ETH Zurich, Switzerland
e-mail: linard.cantieni@igt.baug.ethz.ch

p_∞	Final rock pressure acting upon the lining far behind the face
$p(y)$	Rock pressure acting upon the lining at the axial coordinate y
r	Radial co-ordinate (distance from tunnel axis)
s	Round length in the step-by-step calculations
t	Time
$t_{95\%}$	Time needed in order to reach 95% of the time-dependent deformations
u	Radial displacement of the ground
u_C	Radial convergence of the opening
u_C^e	Elastic part of the radial convergence of the opening
u_C^p	Plastic part of the radial convergence of the opening
u_j	Radial displacement of the ground at point j
u_{oe}	Amount of over-excavation in case of a yielding support
u_y	Axial displacement
u_∞	Final radial displacement of the ground occurring far behind the face
$u(y)$	Radial displacement of the ground at the axial coordinate y
$\bar{u}$	Radial displacement (unsupported opening)
v	Advance rate of the excavation
y	Axial co-ordinate (distance behind the tunnel face)
y_j	Axial co-ordinate of point j

Greek symbols

ΔR	Overcut between excavation and shield
Δp_j	Increase of pressure over the integration interval j
$\dot{\varepsilon}_{ij}$	Strain rate tensor
$\dot{\varepsilon}_{ij}^e$	Elastic part of the strain rate tensor $\dot{\varepsilon}_{ij}$
$\dot{\varepsilon}_{ij}^p$	Inelastic part of the strain rate tensor $\dot{\varepsilon}_{ij}$
η	Viscosity
λ	Stress relief factor
v	Poisson's ratio of the ground
σ_o	Initial stress
σ_{ij}	Stress tensor
σ_{rr}	Radial stress
ϕ	Angle of internal friction of the ground
ψ	Dilatancy angle of the ground

1 Introduction

Under certain conditions which are frequently encountered in tunnel design, the computational models in common use predict that a poor-quality ground will be more favourable for tunnel construction than a high-quality ground. More specifically, the models suggest that a ground of higher strength develops a greater load upon the lining than the load developed by a low-strength ground (all of the other parameters being equal). This is clearly contrary to the behaviour that might be expected both intuitively and on the basis of tunnelling experience, which is that overstressing of the lining or severe convergences are associated with ground of poor quality (e.g. Kovári and Staus 1996). The model behaviour deserves to be called a paradox, i.e. "a seemingly absurd or contradictory statement or proposition which when investigated may prove to be well founded or true" (Oxford Dictionary).

The paradox has been mentioned in passing in a number of older works dealing with the elasto-plastic analysis of tunnels (Nguyen-Minh and Corbetta 1992, p. 86; Nguyen-Minh and Guo 1993, p. 176; Guo (1995), p. 90). More recently, it has been noted by Boldini et al. (2000) and Graziani et al. (2005), who obtained "unforeseen results" from axisymmetric elasto-plastic numerical analyses of advancing tunnels, and explained them by means of the convergence–confinement method ("The decrease in the loading in the plastic case is caused by the increased convergence u_0 before the installation of the lining, which overshadows the negative effect of the flattening of the convergence curve in the plastic range"). Also, Mair (2008) drew basically the same conclusion when discussing the results of plane strain analyses ("This is because the weaker ground leads to higher deformations occurring ahead of the face prior to installation of the lining; the consequence of more ground deformation before installation is a smaller pressure induced on the lining"). Furthermore, Ramoni and Anagnostou (2010b) and Lavdas (2010) observed the counter-intuitive behaviour of the models with respect to the loading of TBM shields and of segmental linings, respectively.

Although the paradox has been noted by a number of authors, it is, interestingly, neither widely appreciated nor well understood in the broader engineering and scientific community. It may therefore perplex the tunnel engineer and raise doubts as to the predictive power of standard tunnel design calculations, which makes it deserving closer investigation. This shall be attempted in the present paper.

Section 2 illustrates the paradox by means of results obtained from the application of commonly used computational methods, investigating the conditions under which the paradox occurs and explaining why the paradox occurs. The computational methods in question are the convergence–confinement method (CCM) for the classic, rotationally symmetric, plane-strain tunnelling problem; the plane strain numerical analysis for tunnels with an arbitrary cross-section; and the axisymmetric analysis for deep cylindrical tunnels. All of these methods exhibit the paradox with respect to the rock loading developing upon a stiff lining that is installed close to the face (the higher the rock strength, the higher the load), but predict the expected

behaviour with respect to convergences (the higher the rock strength, the smaller the convergence).

Even if the reason for the low load predicted in the case of low-strength ground is understood (as mentioned above, it is the stress relief associated with the yielding of the core ahead of the tunnel face), a question remains as to why such behaviour is not exhibited in nature or, in other words: what are the specific modelling assumptions that lead to the paradoxical model behaviour. The main part of the paper deals with these issues. Section 3 outlines possible reasons for the discrepancy between model behaviour and actual behaviour on the basis of qualitative factors, while Sects. 4–8 investigate some of these possible reasons quantitatively and in depth. Putting it in a nutshell, the paradoxical behaviour seen in the model is associated with the commonly made simplifying design assumptions that ground behaviour is time-independent (while in reality the ground generally creeps, particularly in the case of squeezing) and that the support operates with full stiffness close to the face (while in reality the sequence of excavation and support installation is such that deformations inevitably occur).

2 Unexpected Model Behaviour

2.1 Convergence–Confinement Method

The convergence–confinement method (CCM) allows the ground pressure to be assessed by means of closed-form solutions, and is widely used in engineering practice for preliminary dimensioning of the lining (Panet 1995). The method applies to the rotationally symmetric problem of a deep, uniformly supported, circular tunnel crossing a homogeneous and isotropic ground which is subject to uniform and hydrostatic initial stress. Under the additional simplifying assumption of plane strain conditions, the problem becomes one-dimensional (i.e. all field variables depend solely on the distance r from the tunnel axis) and can be solved analytically. The solution can be presented in the form of a so-called "ground response curve", which shows the relationship between the support pressure and the radial displacement of the tunnel boundary. The equations for the case of linearly elastic and perfectly plastic ground behaviour according to the Mohr–Coulomb yield criterion with a non-associated flow rule (which is the material model assumed throughout the present Paper) can be found, inter alia, in Anagnostou and Kovári (1993). Figure 1a shows the ground response curves for an example with the parameters of Table 1 and an uniaxial compressive strength f_c of 1 or 3 MPa.

The CCM investigates the interaction between ground and tunnel support graphically by plotting the ground response curve and the characteristic line of the lining in one and the same diagram. The latter shows the dependency of the radial displacement of the lining on the ground pressure acting upon the lining. The inclination of the characteristic line of the support depends on its stiffness k, while the origin of the characteristic line on the displacement axis (e.g., Point A in Fig. 1a) accounts for the pre-deformation of the ground, i.e. for the radial displacement that takes place before lining installation at a distance e behind the face. The pre-deformation occurs partially ahead of the tunnel face and partially over the unsupported span. In the computational example of Fig. 1a, the simplifying assumption was made that the pre-deformation $u(e)$ follows the longitudinal displacement profile proposed by Chern et al. (1998):

$$u(e) = \bar{u} \left(1 + \exp\left(-0.91\frac{e}{a}\right) \right)^{-1.7}, \tag{1}$$

where $\bar{u}$ and a denote the final unsupported convergence (i.e. the convergence that would occur in an unsupported tunnel far behind the face) and the tunnel radius, respectively. Figure 1a shows the characteristic lines of the lining for support installed directly at the tunnel face ($e = 0$, $u(e)/\bar{u} = 30\%$, dashed lines) or at a distance of $e = 3$ m behind the face ($u(e)/\bar{u} = 50\%$, solid lines).

The intersection point of the ground response curve and of the characteristic line (e.g. Point B in Fig. 1a) satisfies the conditions of equilibrium and compatibility and shows the ground pressure and deformation. It can be seen immediately from Fig. 1a that, as a consequence of the smaller pre-deformations, the predicted ground pressure is higher in the case of a higher strength ground. This is clearly contrary to what one might expect intuitively. Figure 1b provides a more complete picture of the effect of ground strength f_c on final lining pressure.

In view of the paramount effect of pre-deformation on the final lining pressure, the question arises as to whether this unexpected model behaviour might be due to the simplifying assumption of Eq. 1, according to which the pre-deformation amounts to a constant fraction of the final unsupported convergences (i.e. a fraction which is the same for an elastic and for a highly stressed ground). A similar behaviour can be observed when applying the improved longitudinal displacement profiles proposed Vlachopoulos and Diederichs (2009), which in contrast to Chern et al. (1998) consider the maximum plastic radius. The paradox persists even when applying the most advanced method of pre-deformation estimation, which is the so-called implicit method introduced by Nguyen-Minh and Guo (1996) and proposed, inter alia, by AFTES (2002). This method takes into account the lining stiffness and installation point in addition to the properties of the ground and to the extent of the plastic zone. A synopsis of the equations can be found in Cantieni and Anagnostou (2009a). As can be seen from
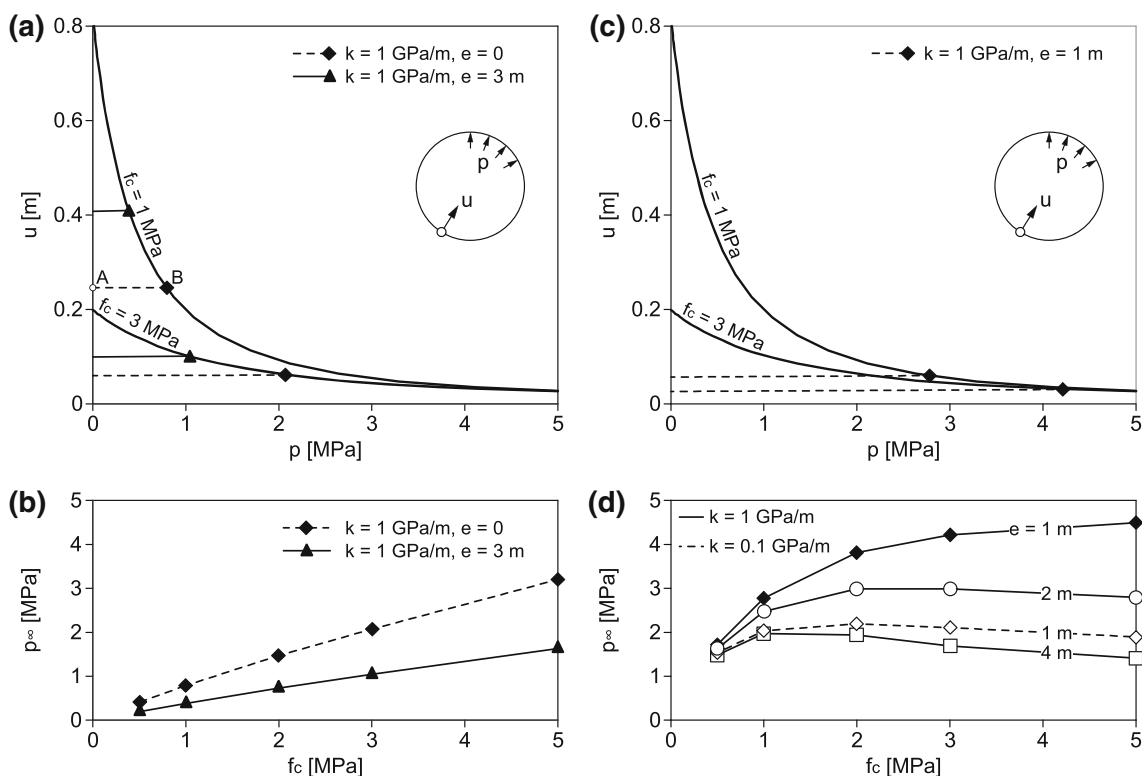
Fig. 1 Determination of the final lining pressure by the CCM for different values of the uniaxial compressive strength of the ground f_c, of the unsupported span e and of the radial stiffness of the lining k. **a** Ground-support interaction (pre-deformations according to Chern et al. 1998); **b** Final lining pressure as a function of the uniaxial compressive strength (pre-deformations according to Chern et al. 1998); **c** Ground-support interaction (pre-deformations according to the implicit method); **d** Final lining pressure as a function of the uniaxial compressive strength (pre-deformations according to the implicit method)

Table 1 Model parameters

Parameter	Value	
Initial stress, σ_0	10 MPa	
Tunnel radius, a	4 m	
Unsupported span, e	Variable	
Ground		
Young's modulus, E	1 GPa	
Poisson's ratio, v	0.3	
Angle of internal friction, φ	25°	
Dilatancy angle, ψ	5°	
Uniaxial compressive strength, f_c	Variable	
Lining		
Radial stiffness, k	1 GPa/m	0.1 GPa/m
Young's modulus, E_L	30 GPa	10 GPa
Thickness, d	0.53 m	0.16 m

the ground–support interaction diagram of Fig. 1c, even this more sophisticated analysis method predicts that the load developing in the case of a ground having an uniaxial compressive strength of $f_c = 1$ MPa is lower than in the case of $f_c = 3$ MPa.

Figure 1d shows the results of a parametric study (performed with the CCM in combination with the implicit method) on the effect of ground strength f_c on final loading at different values of the unsupported span e and of the lining stiffness k. It is interesting to note that the softer the lining and the bigger the unsupported span, the less pronounced is the paradox. In conclusion, the reasons for this will be discussed later in Sect. 2.3.

2.2 Numerical Plane Strain Analysis

One might argue that the paradox described above may be interesting from a theoretical point of view, but is of minor importance in practical terms because the CCM is anyway an oversimplified analytical tool. The purpose of this section is to emphasize that the fundamental principles of the CCM and the conclusions of the last Section apply also to the numerical plane strain analyses that are widely used for design purposes in engineering practice.

For the sake of simplicity and without loss of generality, let us consider again a deep-seated tunnel excavated full face under the same conditions as in the previous section (including Table 1, with the lining characteristics

according to the last column). The only difference is that the tunnel cross-section is no longer circular, with the consequence that rotational symmetry is lost and the problem has to be solved numerically by the finite element method. In order to explain why the paradox persists, let us consider how a numerical plane strain analysis proceeds in such a case. In a plane strain analysis, the three-dimensional tunnel problem is simulated by considering a series of sections normal to the tunnel axis (e.g. Panet 1995). In the case of full face excavation, the computation consists of three steps.

The first step concerns the initial state ("State 0"), which prevails far ahead of the face. Depending on the available computer code, the initial stress field may be either defined or calculated.

The second step simulates the development of pre-deformations during the transition from the initial state to the state prevailing immediately before lining installation ("State 1") by reducing the radial stresses (as well as the shear stresses in the case of a non-hydrostatic initial stress field) acting on the tunnel boundary from their initial value σ_0 to the fictitious internal pressure p_I which simulates the supporting effect of the core. The amount of stress relief is usually expressed by the stress relief factor λ ($0 \le \lambda \le 1$):

$$p_I = (1 - \lambda)\sigma_0. \tag{2}$$

A value of $\lambda = 1$ (complete stress relief) applies to the case of an unsupported tunnel, while $\lambda = 0$ (no stress relief) applies to the theoretical case where support is installed *before* excavation. The stress relief factor governs the amount of pre-deformation, accounts for the stiffness and for the installation point of the support and is estimated by one of the methods mentioned in the previous section. Figure 2 shows the stress relief factor λ (calculated according to the implicit method for the parameter values of Table 1) as a function of the uniaxial compressive strength f_c. The lower the ground strength, the more pronounced will be the yield of the core ahead of the face, the higher will be the stress relief factor λ and, consequently (cf. Eq. 2), the lower will be the fictitious internal pressure p_I.

The third step simulates the transition from State 1 to the final state prevailing far behind the face ("State 2") by activating the finite elements that simulate the support and by setting the tractions at the tunnel boundary equal to zero. The resulting values include the final displacement and rock load as well as the lining forces (bending moments and hoop forces). A stiff lining that is installed close to the face prevents the development of further convergences and thus further stress relief. As a consequence, the final lining loading practically corresponds to the radial stress prevailing at the tunnel boundary at State 1, i.e. to the internal pressure p_I, which, as mentioned
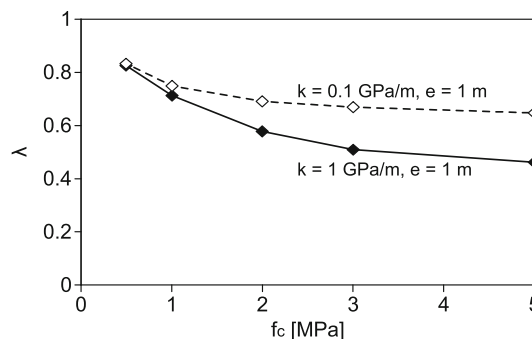

Fig. 2 Stress relief factor λ as a function of the normalized uniaxial compressive strength f_C/σ_0 for the radial stiffness of the lining k of 0.1 and 1 GPa/m (other parameters according to Table 1)

above, decreases with the strength of the ground. The consequence is that a weak ground develops a lower loading.

Figure 3 shows, as an example, the numerical results obtained by the FEM code PLAXIS (Brinkgreve 2002) for a non-circular tunnel with the model parameters of Table 1 (lining data according to the last column). The stress relief factors were taken from Fig. 2 with a stiffness $k = 1$ GPa/m. The calculated bending moments and axial forces (although not manageable structurally) also illustrate the existence of the paradox. The paradox thus applies not only to analytical solutions that incorporate many simplifications, but also to the widely used numerical plane strain computational method.

2.3 Numerical Axially Symmetric Analysis

On account of the uncertainties introduced by the simplifying assumptions of plane strain analyses with respect to pre-deformation (which, as discussed above, is a very important parameter), it is reasonable to ask whether the paradox is a problem specifically of the plane strain model or if it also occurs in spatial (i.e., three-dimensional or axisymmetric) analyses which do not involve assumptions about convergences ahead of the face. An additional reason for raising this question is that plane strain analyses, in contrast to spatial calculations, do not correctly reproduce the actual stress history of the ground, and this may influence the results not only quantitatively, but also qualitatively (Cantieni and Anagnostou 2009a, b).

Let us therefore investigate the behaviour of the axially symmetric model of a deep cylindrical tunnel. The problem setup is exactly the same as in Sect. 2.1, the only difference being that we no longer make the plane strain assumption. The problem is solved numerically by the so-called "steady state method", a method introduced by Nguyen-Minh and Corbetta (1991) for efficiently solving problems with constant conditions in the tunnelling direction by considering a
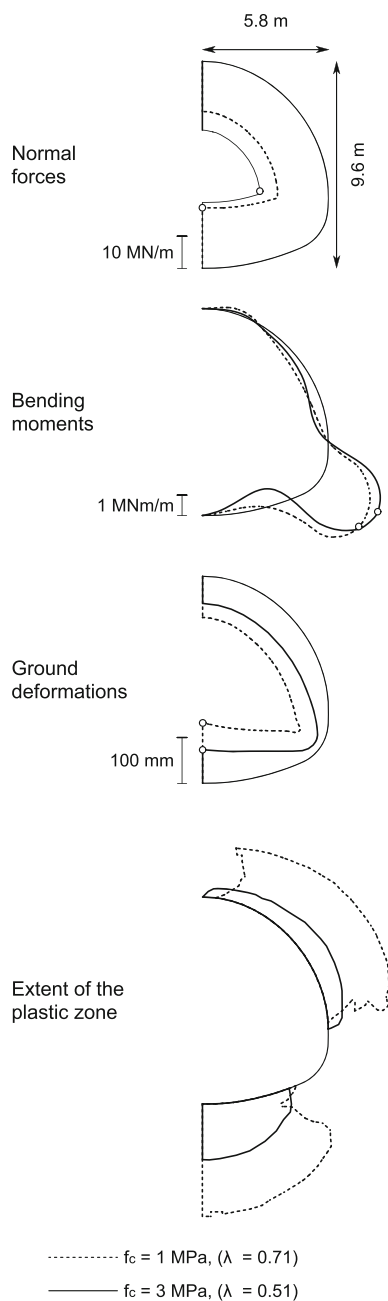
5.8 m

9.6 m

Normal
forces

10 MN/m

Bending
moments

1 MNm/m

Ground
deformations

100 mm

Extent of the
plastic zone

·········· fc = 1 MPa, (λ = 0.71)
———— fc = 3 MPa, (λ = 0.51)

Fig. 3 Numerically determined distribution of the **a** hoop force N,
b bending moment M, **c** deformation of the tunnel boundary u and
d extent of the plastic zone for two values of the uniaxial compressive
strength f_c

reference frame, which is fixed to the advancing tunnel face.
A comparison of the steady state method with the more
widely used "step-by-step method", which handles the
advancing face by deactivating and activating the ground
and support elements, respectively, was presented recently
in this Journal by Cantieni and Anagnostou (2009a). As
discussed by the Authors, the steady state method applies to
the borderline case of continuous tunnel advance (round
length $s = 0$).

Figure 4a shows the model. The lining is modelled as an
elastic radial support with stiffness $k = dp/du$, where p and
u denote its radial loading and radial displacement,
respectively. The radial stiffness k of a ring-shaped lining
is equal to $E_L d/a^2$, where a, d, and E_L denote its radius,
thickness, and Young's modulus, respectively. The longi-
tudinal bending stiffness of the lining will not be taken into
account. The lining is installed at a distance e behind the
tunnel face.

Figure 4d shows the development of radial stress at
$r = a$ (which for $y > e$ is identical with the lining loading)
along the tunnel for two values of the uniaxial compressive
strength of the ground f_c. It can be easily seen that—
analogously to the results of the CCM—both the radial
stress ahead of the face and the pressure developing upon
the lining are lower in the case of the lower strength
ground, while the deformations (particularly the ones
occurring ahead of the face) and the extent of the plastic
zone are larger (Fig. 4b, c respectively).

In order to gain more information about the behaviour of
the model, a parametric study was performed on the effects
of ground strength f_c, unsupported length e and lining
stiffness k. Figure 5a and b shows the final lining pressure
p_∞ as a function of the uniaxial compressive strength
f_c (both normalized by the initial stress σ_0) for a stiff and a
soft lining ($k = 1$ and 0.1 GPa/m, respectively). Both
diagrams clearly show the counter-intuitive behaviour (the
load increasing with the ground quality) at unsupported
lengths e up to 2 m. Similarly to the CCM (Sect. 2.1), the
stiffer the lining and the shorter the unsupported span, the
more pronounced is the paradox.

The lower the strength of the ground, the more will the
radial stress in the core ahead of the face decrease and, as
the lining actually undertakes the role of the core after
excavation, the lower will be the lining load. If the strength
of the ground is high, however, the core ahead of the face
will be able to sustain a high radial stress and, as a stiff
lining that is installed close to the face does not allow for
additional deformations and stress relief, a high load will
develop upon the lining. On the other hand, a low stiffness
lining or a long unsupported span allow deformations and
stress relief to develop behind the face (whatever the
strength of the ground) with the consequence that the
paradox becomes less pronounced.

As the convergence of the excavated profile is a directly
observable phenomenon in tunnelling, unlike rock pressure
(and in fact large convergences are what tunnel engineers
associate with poor quality ground), it is interesting to
check the model behaviour also with respect to deforma-
tions. Figure 5c and d shows the convergence u_c of the
excavated section ($u_c = u_\infty - u(0)$) as a function of the
ground strength f_c and of the unsupported span e. It can be
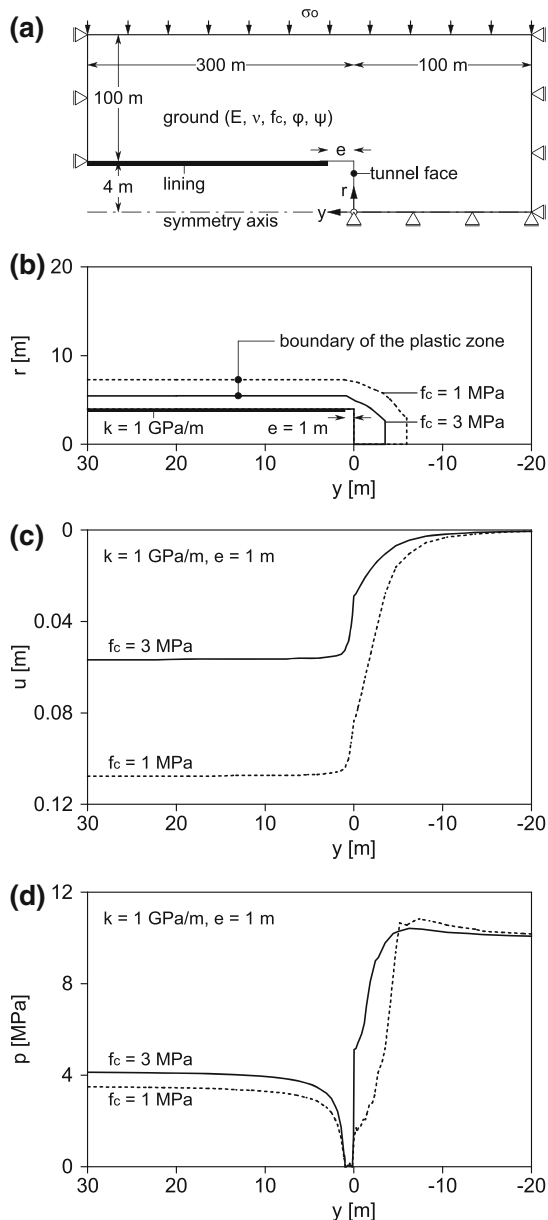seen that the model predictions correspond to expectations:

Fig. 4 **a** Axially symmetric model and boundary conditions; **b** extent of the plastic zone; **c** radial displacement u of the ground at the tunnel boundary; **d** radial stress at the tunnel boundary (for $y > e = 1$ m, the radial stress corresponds to the ground pressure on the lining)

the lower the strength, the larger the convergence. This is true also concerning the convergence of an unsupported tunnel (Fig. 6). The model behaviour is counter-intuitive only with respect to the load developing upon the lining.

3 Reasons for the Discrepancy Between Model and Reality

Although the reason for the unexpected model behaviour is understood, it is still puzzling, why such behaviour is not observed in reality. Obviously there must be one or more modelling assumptions which contradict what happens in reality and which are responsible for the observed difference between model behaviour and actual behaviour. The results of the previous section provide useful indications as to the relevant modelling assumptions.

The finding that the paradox is due to deformations and to the stress relief associated with the plastic yield of the ground *ahead* of the face indicates that the modelling assumptions which provide for this stress relief may be responsible for the paradox. As explained below under points (i) and (ii) there are at least two reasons why the actual deformations of the ground and the stress relief *ahead* of the face may be smaller than in the computational models of Sect. 2 which show the paradoxical behaviour.

The finding that the paradox occurs particularly under the modelling assumption that a stiff lining is installed near the face (and becomes less and less pronounced or disappears when the ground is allowed to converge *behind* the face) indicates that this modelling assumption may be an oversimplification. In fact, there are several sources of deviation between the model and reality which are associated with the development of deformations *behind* the face. These deviations may also explain the difference between the behaviour of the model and actual behaviour, i.e. the absence of the paradox in reality. The deformations *behind* the face may occur intentionally (as in the case of yielding supports, see point (iii) below) or unintentionally, for example due to support destruction (iv), due to the excavation and support installation sequence (v–vii) or due to the early stiffness of the support components (viii). Deformations even occur in cases with a presumably stiff support as in the case of a segmental lining in shield tunnelling (ix).

(i) *Time-dependency of the ground behaviour* The first reason is of a fundamental nature, as it is associated with the rheological properties of the ground. Creep is particularly important in the case of overstressed ground (i.e., when the stresses reach its bearing capacity) and is therefore also important for the question under consideration. In general, plastic yielding develops with a certain delay which is dependent on its rheological properties. The latter, together with the advance rate, are decisive in terms of the extent of plastic yield and the amount of stress relief ahead of the advancing face. The higher the viscosity of the ground and the higher the advance rate, the smaller will be the plastic deformations and the stress relief and the less pronounced will be the paradox (the effect of the ground strength appears with a delay—behind the face). Section 4 confirms this hypothesis by means of numerical computations.
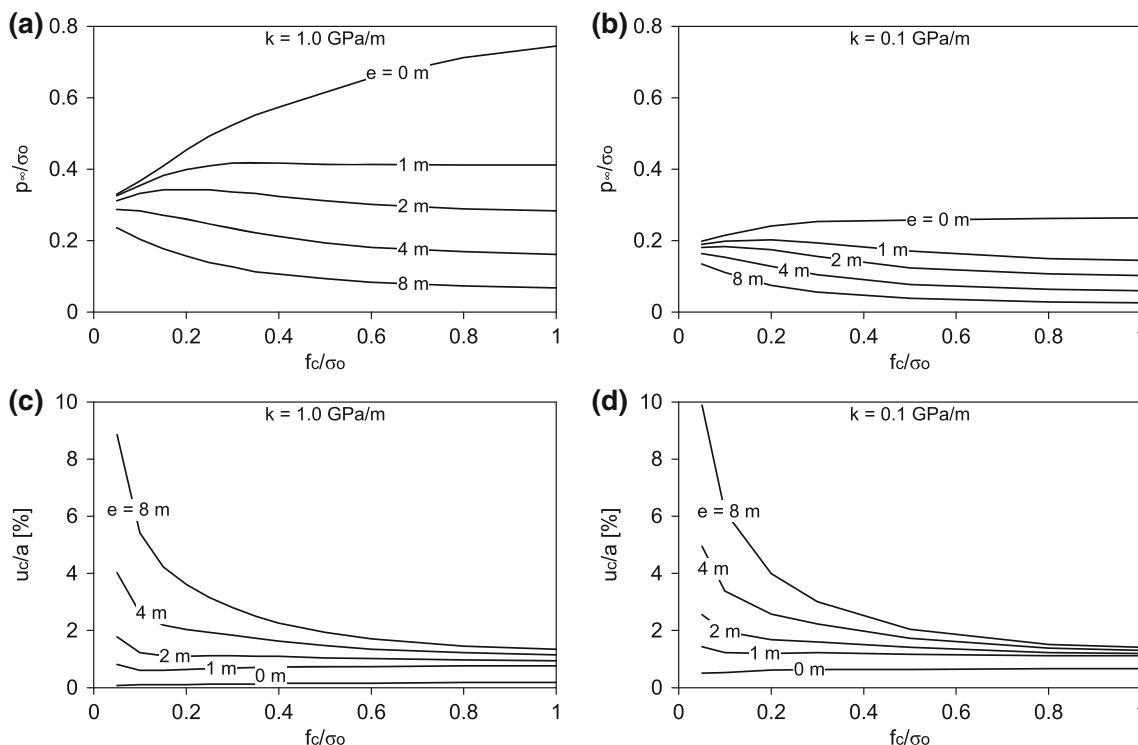
Fig. 5 Effect of the normalized uniaxial compressive strength f_c/σ_0 on the **a** normalized final lining pressure p_∞/σ_0 for a radial lining stiffness k of 1 GPa/m; **b** normalized final lining pressure p_∞/σ_0 for a radial lining stiffness k of 0.1 GPa/m; **c** normalized convergence u_C/a for a radial lining stiffness k of 1 GPa/m; and **d** normalized convergence u_C/a for a radial lining stiffness k of 0.1 GPa/m
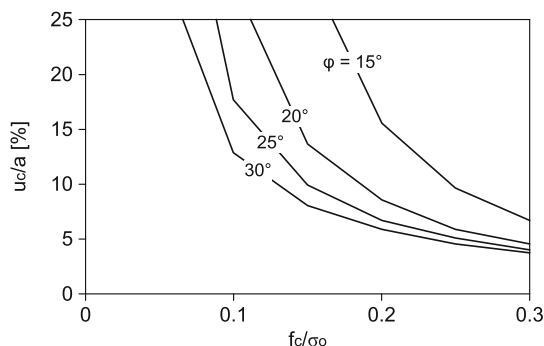

Fig. 6 Normalized radial convergence of an unsupported tunnel u_C/a as a function of the normalized uniaxial compressive strength f_c/σ_0 and of the angle of internal friction φ

(ii) *Face support or reinforcement* The second effect is associated with specific measures that are often applied in weak ground in order to stabilize the face or to limit its extrusion. Face bolting increases the bearing capacity of the core ahead of the face and, as the reinforced core is able to sustain a higher radial stress, limits stress relief. Consequently, the paradox should become less pronounced. Section 5 investigates this hypothesis and shows that the paradox disappears only at very high face support pressures that are barely feasible from a technical perspective.

(iii) *Yielding support* Yielding supports are installed close to the face and allow the ground to converge under an approximately constant pressure. Figure 7 shows the support measures applied in the case of the yielding support developed for the Sedrun Lot of the Gotthard Base Tunnel. As the paradox becomes less pronounced or disappears when the ground is allowed to converge behind the face, it is reasonable to expect that it will not occur in the case of yielding supports. Section 6 confirms this hypothesis quantitatively. The model exhibits the expected behaviour: the higher the strength of the ground, the lower the rock pressure and the smaller the convergence.

(iv) *Damage to the support* Decreasing ground quality in tunnelling is recognized through increasing convergences. In the case of a stiff support, large deformations can only occur if the ground pressure overstresses and damages the lining (Fig. 8). Damaged support offers only a low or zero resistance to deformations. As already discussed (Fig. 6), the model of an unsupported tunnel exhibits the expected behaviour: the convergences increase with decreasing ground strength.

(v) *Partial face excavation* In the case of partial face excavation (e.g. the top heading, bench- and invert-excavation method), the stiffness of the support system is low

Fig. 7 Scheme of the yielding support system realized in the Sedrun Lot of the Gotthard Base Tunnel (after Ehrbar and Pfenninger 1999)
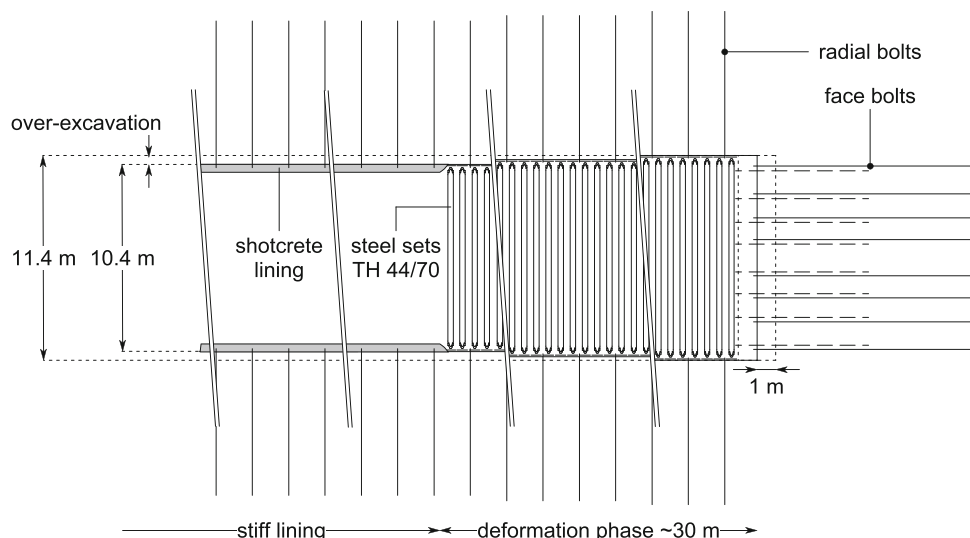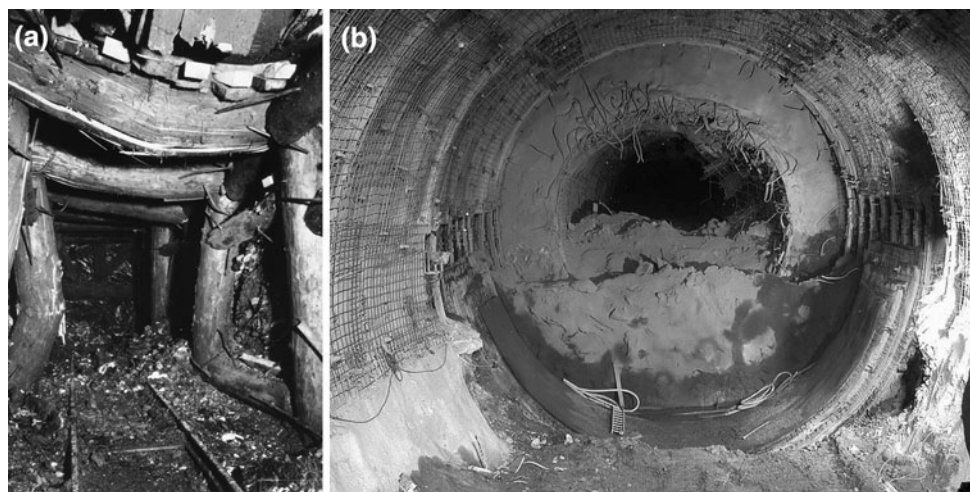

Fig. 8 a Historical picture of a tunnel with damaged wooden support; **b** reshaped cross-section (in the front of the picture) after the support was damaged (in the background of the picture) in the Faido Lot of the Gotthard Base Tunnel (courtesy of AlpTransit Gotthard AG, Switzerland)

before completing the excavation of the cross-section and closing the lining at the invert (A in Fig. 9). The initially low stiffness allows for convergences behind the face, which should reduce or even eliminate the paradoxical behaviour (according to the findings of Sect. 2).

(vi) *Staggered support application* The construction process is usually such that the application of support measures (steel sets, shotcrete, bolts) is staggered along the tunnel alignment (Fig. 7, B in Fig. 9). The stiffness of the support system is initially low and increases with the distance from the face. The ground can thus converge in the regions close to the face, thereby reducing or eliminating the paradoxical behaviour.

(vii) *Unsupported span* According to Fig. 5, the cases with an unsupported span of $e = 0$ yield the most pronounced paradox. In conventional tunnelling, an unsupported span of $e = 0$ is not feasible. Even if all support

components are installed immediately after each excavation round right at the face, the next excavation step ($s > 0$) would temporarily create an unsupported span (C in Fig. 9). Therefore, the modelling assumption of $e = s = 0$ (underlying the curves denoted by $e = 0$ of Fig. 5), which almost entirely prevents the development of convergence behind the face, represents only a theoretical limiting case.

(viii) *Stiffness of green shotcrete* Another possible source of deformations behind the face is the low stiffness of green shotcrete. The final Young's modulus of shotcrete is normally reached only after several days. For high advance rates, the stiffness of the lining is therefore low near the face (D in Fig. 9). Section 7 investigates by means of numerical computations whether the paradox persists when taking this effect into account, and shows that it is a rather minor effect. The counter-intuitive model behaviour disappears only at very high advance rates (>20 m/day).
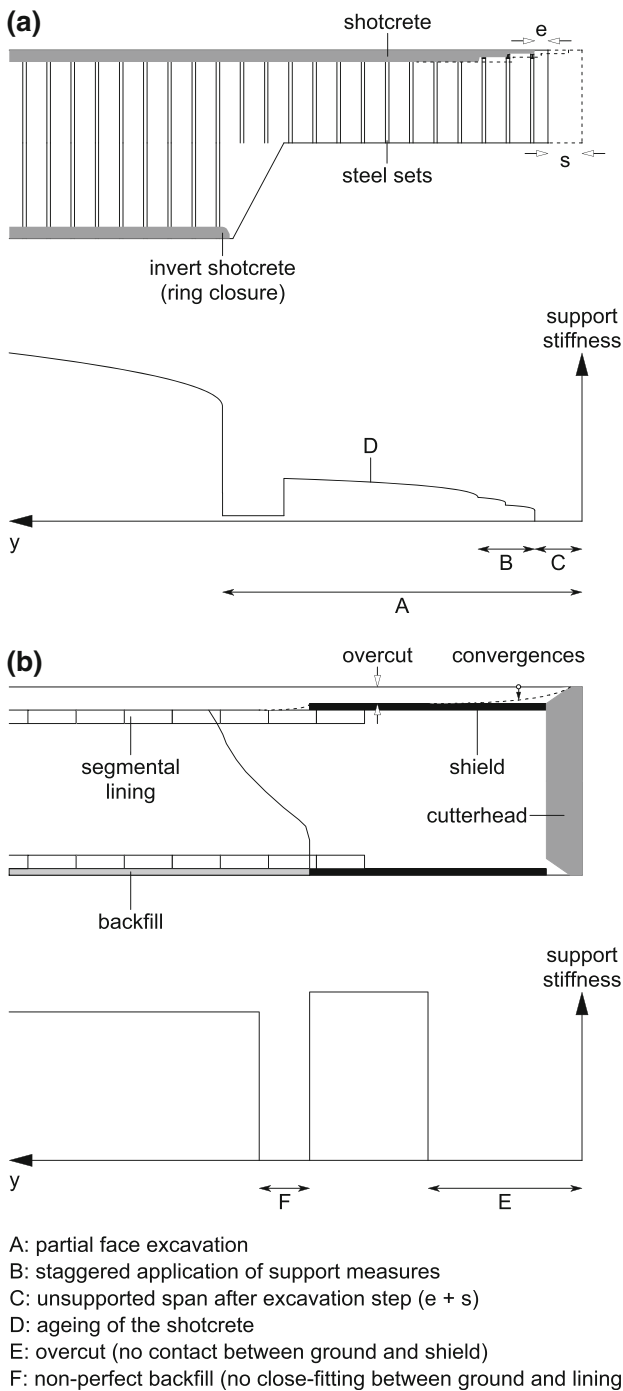
(a)

(b)

A: partial face excavation
B: staggered application of support measures
C: unsupported span after excavation step (e + s)
D: ageing of the shotcrete
E: overcut (no contact between ground and shield)
F: non-perfect backfill (no close-fitting between ground and lining)

Fig. 9 Sources of unavoidable deformations during **a** conventional tunnelling and **b** TBM tunnelling

(ix) *TBM tunnelling* With respect to TBM tunnelling, the assumptions of $e = 0$ (no unsupported span) and $s = 0$ (zero round length), which lead to the most paradoxical model behaviour (Fig. 5), seem at a first glance to be realistic because of the continuous advance of the shield. However, the design of the machines always provides a certain "overcut" ΔR between excavation diameter and

shield extrados, which is needed for steering the machine (and sometimes also for avoiding jamming of the shield). The overcut allows the ground to converge behind the face (E in Fig. 9). Additional deformations may occur behind the shield even in the presence of a stiff segmental lining, depending on the type and on the point of application of the backfill (F in Fig. 9). Section 8 investigates the effects of the overcut in more detail and shows that the overcut reduces or even eliminates the paradoxical behaviour.

4 Effect of Creep

4.1 Computational Model

Time-dependency is taken into account by applying the elasto-viscoplastic creep model after Madejski (1960). The inset in Fig. 10 shows the micro-mechanical model, which consists of an elastic spring in series with a Bingham model. The strain rate $\dot{\varepsilon}_{ij}$ is resolved into an elastic and an inelastic part:

$$\dot{\varepsilon}_{ij} = \dot{\varepsilon}_{ij}^{e} + \dot{\varepsilon}_{ij}^{p}. \tag{3}$$

The elastic part depends linearly on the stress rate (Hooke's law), while the inelastic part $\dot{\varepsilon}_{ij}^{p}$, which represents combined viscous and plastic effects, reads according to the classic formulation of Perzyna (1966) as follows:
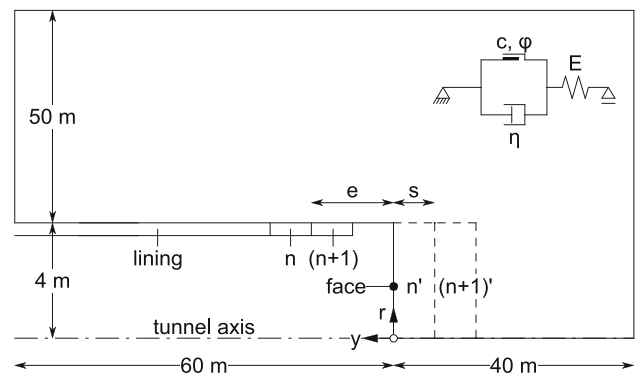
calculation steps:
lining istallation **n**
calculation for excavation **n'** in $\Delta t = 0$
transient calculation with $\Delta t = 1$ day
lining istallation **(n+1)**
calculation for excavation **(n+1)'** in $\Delta t = 0$
transient calculation with $\Delta t = 1$ day
...

Fig. 10 Problem layout and boundary conditions of the step-by-step numerical model including the sequence of the calculation steps and the micro-mechanical material model

Table 2 Response times of a circular unsupported tunnel under plane strain conditions

Viscosity η (kPa day)	$t_{95\%}$
10^3	A few hours to a few days
10^4	A few days to a few weeks
10^5	A few weeks to a few months
10^6	A few months to a few years
10^7	Several years

$$\frac{\mathrm{d}\varepsilon_{ij}^{\mathrm{p}}}{\mathrm{d}t} = \frac{f}{\eta}\frac{\partial g}{\partial \sigma_{ij}}, \qquad (4)$$

where f, g, and η denote the yield function, the plastic potential and the viscosity, respectively. According to this equation, both the deviatoric and the volumetric strains are time-dependent. In contrast to more sophisticated time-dependent constitutive models (e.g. the SHELVIP model, Debernardi and Barla 2009, and the CVISC model, Itasca 2006), the instantaneous response of the assumed material model is purely elastic.

As the development of plastic deformations takes time, the extent of the plastic zone ahead of the tunnel face and the magnitude of the pre-deformations also depend on the advance rate. It is easy to show (by means of a dimensional analysis) that the response of the model depends on the product of the advance rate v and the viscosity η (c.f. Bernaud 1991). The effect of a high advance rate is equivalent to that of a high viscosity. In the borderline case of an "infinitely" rapid excavation, only elastic deformations will occur around the advancing face. In general, the lower the advance rate, the larger will be the plastic deformations.

The ground pressure developing upon the lining is determined by means of a transient stress analysis based on an axially symmetric model (Fig. 10). The tunnel advance is simulated with 60 excavation steps, each containing an instantaneous advance of $s = 1$ m, followed by a transient calculation covering a period of 1 day (overall advance rate $v = 1$ m/day). Figure 10 shows the sequence of excavation and support installation. After 60 steps, tunnel advance is halted and a transient analysis is performed in order to study the development of deformations and rock pressures during the standstill. The analysis stops when a steady state is reached, i.e. when the extrusion rate of the face becomes very small.

For the purpose of comparison, we also carried out time-independent elasto-plastic computations ($\eta = 0$). In contrast to Sect. 2.3, the time-independent problem of the present section was also solved by the step-by-step method,

in order to eliminate the effect of the round length s, which is equal to zero in the steady state method.

The calculations have been carried out with the parameters of Table 1, an unsupported span of $e = 1$ m and various viscosity values. Table 2 gives a sense of the numerical values of viscosity η (a less familiar material constant) by making reference to the response of the relatively simple model of a circular unsupported tunnel under plane strain conditions. The time $t_{95\%}$ denotes the period that must elapse in order that the time-dependent convergence reaches 95% of its final value. Details can be found in the Appendix A.

4.2 Model Behaviour

Figure 11a and b shows the pressure distribution upon the lining for elasto-plastic ($\eta = 0$) and elasto-visco-plastic ($\eta = 10^6$ kPa day) ground behaviour, respectively, and for two values of the uniaxial compressive strength f_c. In contrast to elasto-plastic ground, elasto-viscoplastic ground responds as expected (the load increases with decreasing ground strength). The reason for the model behaviour becomes evident if we consider the radial deformations in the ground ahead of the face (Fig. 11c, d). In contrast to elasto-plastic ground, the radial deformations ahead of the face and thus also the stress relief in elasto-viscoplastic ground depend only slightly on the ground strength f_c, because the short-term response is mainly elastic for the assumed advance rate and viscosity.

Figure 12 shows the results of a parametric study into the effects of viscosity η and ground strength f_c on the lining pressure developing at a distance of five tunnel diameters behind the face. It can be seen that the paradox ceases to exist at viscosities $\eta \geq 10^5$ kPa day, i.e. when the response of the ground to tunnelling takes at least a few weeks (Table 2). Such a slow response is nothing unusual. For example, Fig. 13a–c shows the time-development of the face extrusion measured during excavation standstills at some cross-sections in the northern stretch of the Sedrun Lot, which is part of the new Gotthard Base Tunnel. The deformations develop within a period of 1 week to 1 month. The convergences recorded in the Saint Martin La Porte tunnel show that the transient process may even continue for several months (Fig. 13d).

In conclusion, as a consequence of the time-dependency of the ground response, the stress relief ahead of the face may be much less pronounced than predicted by the simplified time-independent computational models. This is sufficient to make the paradox disappear.
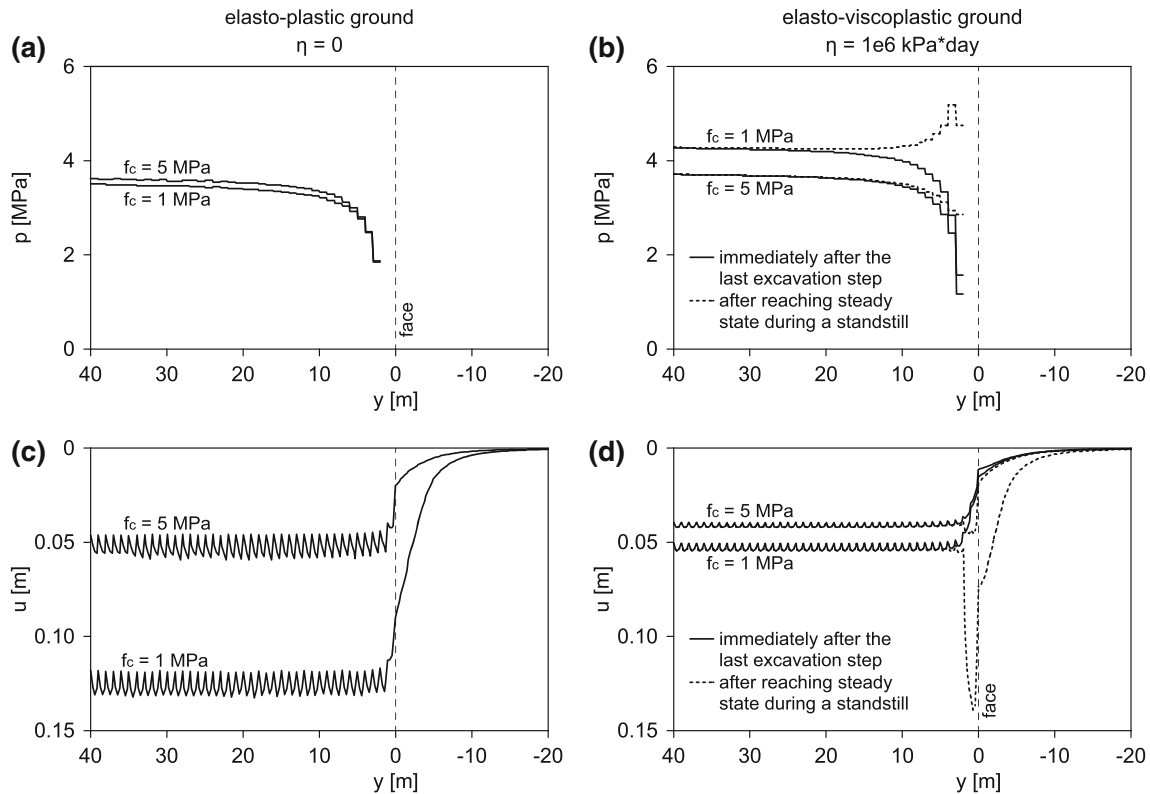
Fig. 11 Development of ground pressure along the tunnel **a** for elasto-plastic ground with time-independent response, **b** for an elasto-viscoplastic ground. Radial convergences along the tunnel **c** for elasto-plastic ground with time-independent response, **d** for an elasto-viscoplastic ground (c.f. Gioda and Cividini 1996)
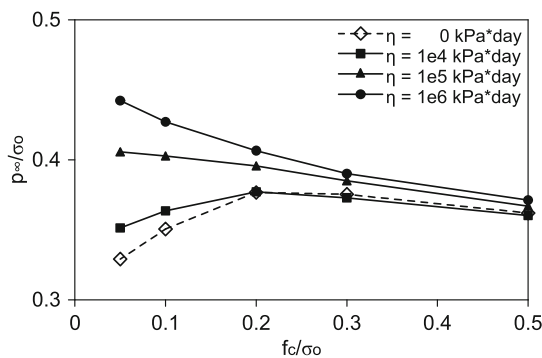

Fig. 12 Normalized final pressure on the lining p_∞/σ_0 as a function of the normalized uniaxial compressive strength f_c/σ_0 and of the viscosity η

5 Effect of Face Reinforcement

5.1 Computational Model

The effect of face reinforcement on the extrusion of the core has been studied intensively for shallow (e.g. Wong et al. 2004; Peila 1994) and also for deep tunnels (e.g. Oreste et al. 2004). The reinforcement provides an additional confinement for the ground in an axial direction, which increases the bearing capacity of the core, i.e. its

ability to sustain a radial pressure, and therefore reduces the stress relief, which, as discussed in Sect. 2, is the main cause of the counter-intuitive behaviour.

The quantitative investigation of these effects is based upon the axially symmetric model of Fig. 4a. The face reinforcement is taken into account in a simplified manner by prescribing a uniform pressure p_F to the face (cf. inset of Fig. 14).

5.2 Model Behaviour

Figure 14 shows the ground pressure developing upon the lining in the final state far behind the tunnel face as a function of the normalized ground strength f_c and of the normalized face support pressure p_F. The higher the face support pressure, the higher will be the final load. The model behaviour agrees with the results of Boldini et al. (2000) and Kasper and Meschke (2006), but does not seem to support the hypothesis formulated by Lunardi (2000), which postulates that the stresses on the lining are lower when the advance core is reinforced.

As expected on the basis of qualitative factors, the paradox becomes less and less pronounced with increasing face pressure and disappears at pressures p_F higher than 0.1–0.2 σ_0. This threshold value is not feasible in the case
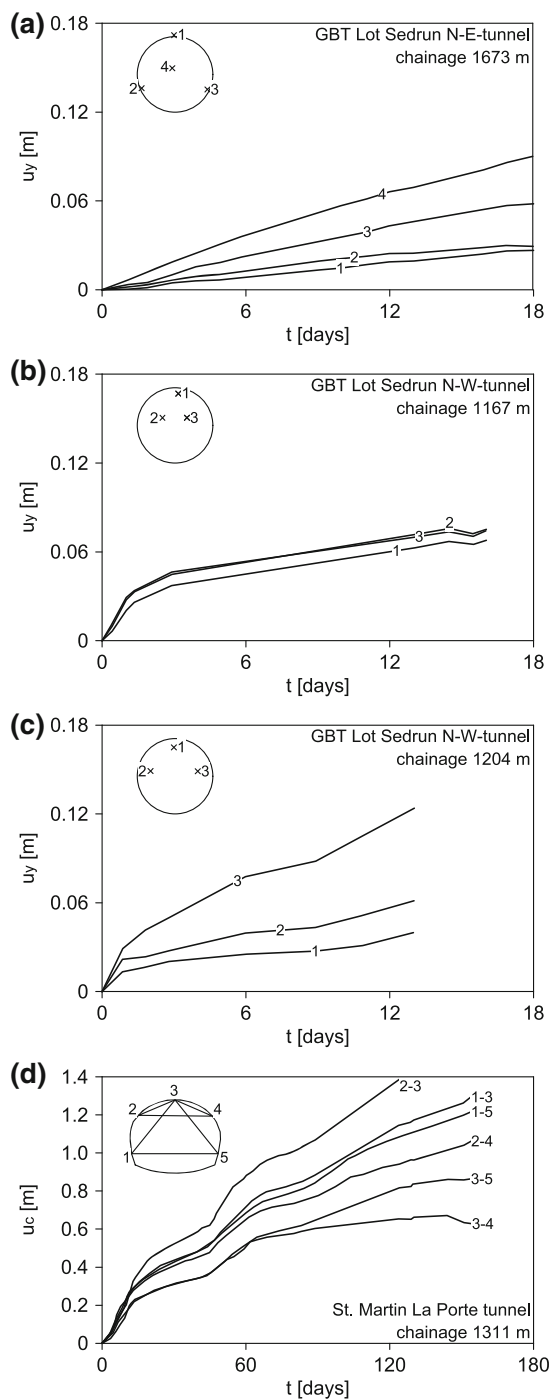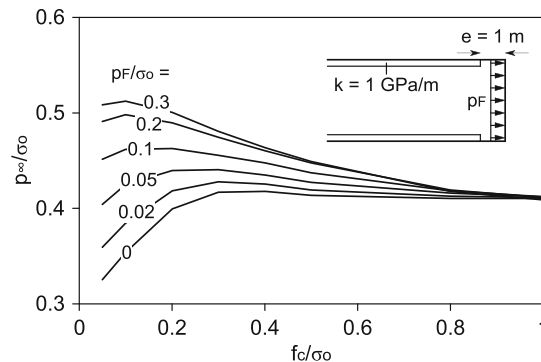
Fig. 14 Final lining load p_∞ as a function of the uniaxial compressive strength f_c and of the face support pressure p_F (all values normalized by the initial stress σ_0)

cover should be smaller than about 100 m. Face reinforcement is of secondary importance as far as the topic of the present paper is concerned.

6 Effect of Yielding Support

6.1 Computational Model

The present section investigates whether the deformations behind the face, which occur intentionally by means of a yielding support, eliminate the paradox. For the purpose of the present investigation, the mixed boundary condition presented in the recent paper of Cantieni and Anagnostou (2009b) will be applied in order to map the complete behaviour of the yielding support system. The response of the yielding support to loading can be approximated by a tri-linear characteristic line (Fig. 15a). The first part of the characteristic line is governed by the stiffness k_I of the system up to the onset of yielding. The second part of the line corresponds to the phase, where the support system deforms under a constant pressure p_y. When the amount of over-excavation u_{oe} is used up, the third phase is initialized. The system is made practically rigid (stiffness k), e.g. by applying shotcrete, with the consequence that an additional pressure accumulates upon the lining. A yielding support which consists of sliding steel sets placed every 0.5 m, each offering a sliding hoop resistance of 800 kN (four friction loops offering a sliding resistance of 200 kN each), will provide a yielding support pressure p_y equal to 400 kPa. After the over-excavation gap is used up, a shotcrete lining is placed, which offers a stiffness k of 1 GPa/m. The stiffness k_I is of subordinate importance for the final ground pressure and is taken as 1 GPa/m. With the exception of this boundary condition, the numerical model is the same as previously (Fig. 4a).
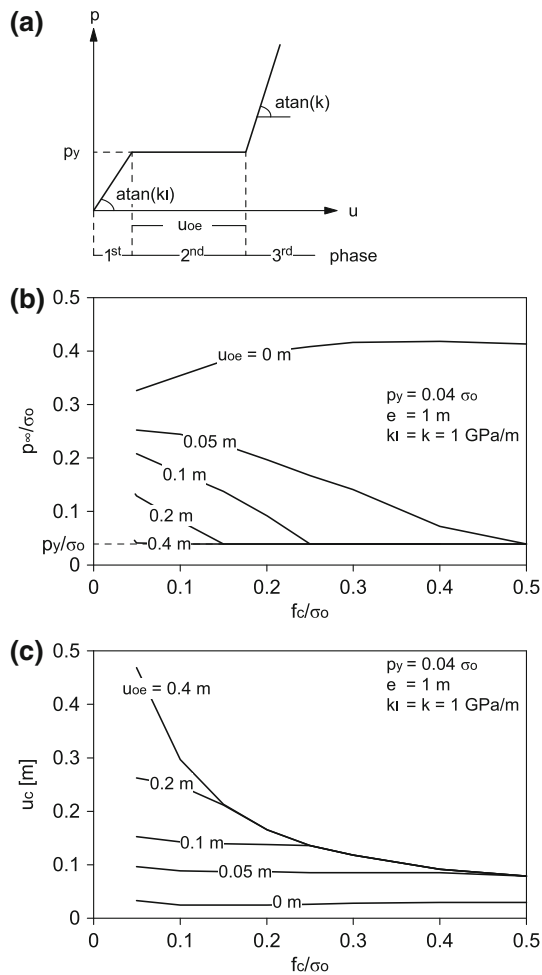

Fig. 13 Time-development, **a–c** of the face extrusion u_y in the Sedrun Lot of the Gotthard Base Tunnel (courtesy of AlpTransit Gotthard AG, Switzerland) and, **d** of the convergence u_c in the Saint Martin La Porte tunnel (Barla et al. 2008)

of deep tunnelling under a high initial stress σ_0. Consider, for example, a heavy face support consisting of one 300 kN bolt per sqm, thus providing a face pressure p_F of 0.3 MPa. In order that the normalized face support pressure p_F/σ_0 is higher than the threshold value of 0.1–0.2, the depth of

(a)

(b)

(c)

Fig. 15 Normalized convergence u_c/a as a function of the normalized uniaxial compressive strength f_c/σ_0 and of the normalized yield pressure p_y/σ_0 of the support

6.2 Model Behaviour

Figure 15b shows the ground pressure developing upon the lining in the final state far behind the tunnel face as a function of the normalized ground strength f_c and of the amount of over-excavation u_{oe}. The upper line ($u_{oe} = 0$) denotes a rigid support installed 1 m behind the face (c.f. line $e = 1$ m in Fig. 5a) and shows the paradox. If a very small theoretical over-excavation u_{oe} of 0.05 m is applied, the paradox disappears. In the present example, the over-excavation will not be used up completely in the case of high amounts of over-excavation. Consider, for instance, an over-excavation of 0.4 m. The final rock pressure acting upon the lining is equal to the yielding support pressure p_y for all ground strengths, because the over-excavation is not used completely and thus the third phase of the system is not reached. (For a detailed analysis of the interaction between yielding supports and ground see Cantieni and Anagnostou 2009b). Figure 15c shows the convergences of the opening u_C (sum of the

convergences of the support and the convergences over the unsupported span) as a function of the normalized ground strength f_c. The deformations also show an intuitive behaviour: lower convergences for increasing ground quality, particularly for cases where the over-excavation is not used up.

In summary, the model of a tunnel with yielding support shows an intuitive behaviour for both the rock pressure on the lining and the ground convergences.

7 Effect of the Low Stiffness of Green Shotcrete

7.1 Computational Model

In general, a shotcrete lining develops its stiffness over time and reaches its long-term stiffness a certain distance behind the face. The assumption of a stiff shotcrete lining right from the start is valid only for low advance rates. The higher the advance rate, the newer will be the shotcrete and the lower its resistance to ground deformations in the vicinity of the face. The time-dependent interaction between shotcrete and the ground has been investigated, e.g. by Graziani et al. (2005), Oreste (2003), Boldini et al. (2005) and Pöttler (1990). In the present section we focus on the question of whether the paradox (which, as stated in Sect. 2, is particularly pronounced in the case of stiff linings) persists when taking into account the initially low stiffness of green shotcrete.

In our computations, the time-dependency of the Young's modulus of shotcrete $E_L(t)$ is taken into account by adopting the empirical relationship of Chang (1994):

$$E_L(t)/E_{L,28} = 1.062 \ \exp\left(-\frac{0.446}{t^{0.6}}\right), \tag{5}$$

where $E_{L,28}$ denotes the Young's modulus of shotcrete at 28 days (taken to 30 GPa in the present case) and t is the shotcrete age in days. Figure 16a shows the evolution of the normalized Young's modulus of the shotcrete over the time, while Fig. 16b, which is nothing more than a simple transformation of Fig. 16a, shows the distribution of the Young's modulus along the tunnel for advance rates of 1, 8, and 20 m/day.

Again, the axially symmetric numerical model of Fig. 4a is used and the problem is solved by the steady state method. The time-dependency of the shotcrete stiffness (Fig. 16a) or the spatial variation of the stiffness along the tunnel (Fig. 16b) is taken into account numerically by considering a series of superimposed lining layers (see Appendix B for details).

7.2 Model Behaviour

Figure 17 illustrates the effect of the advance rate v on the distribution of ground pressure along the tunnel for a lower
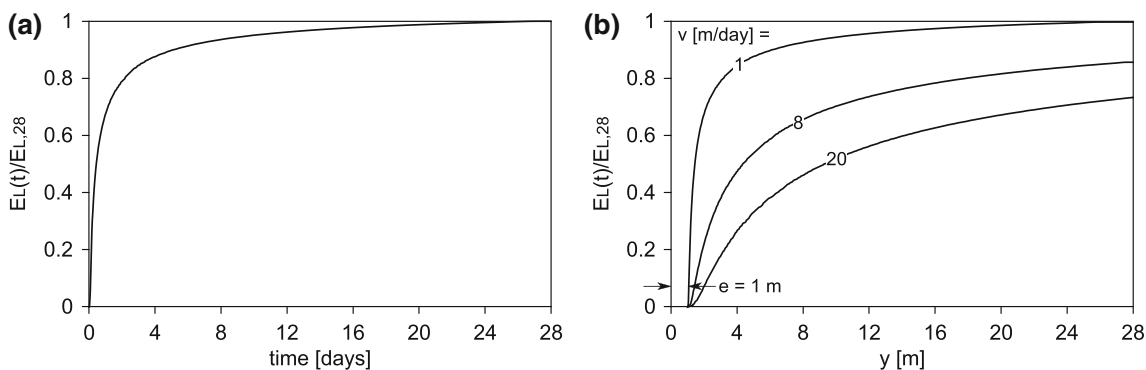
Fig. 16 **a** Time-development of the Young's modulus of the shotcrete after Chang (1994); **b** Normalized Young's modulus of the shotcrete as a function of the distance from the face and of the advance rate v
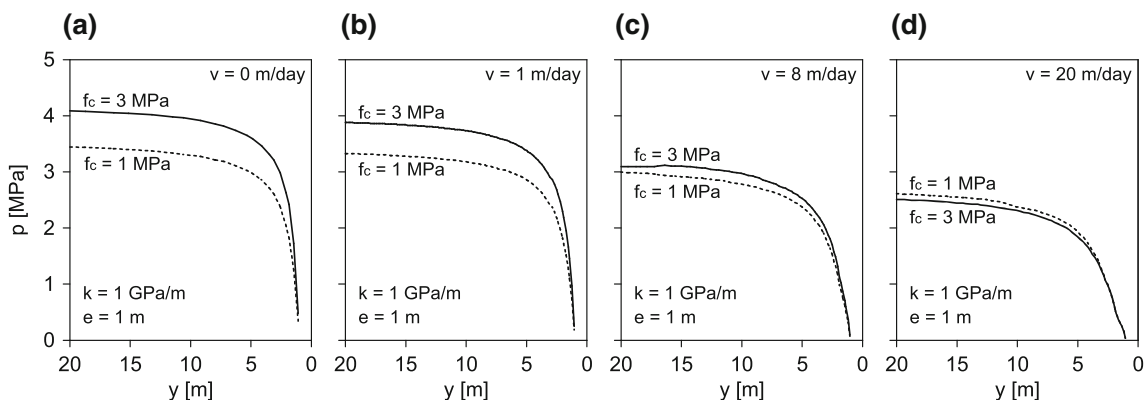

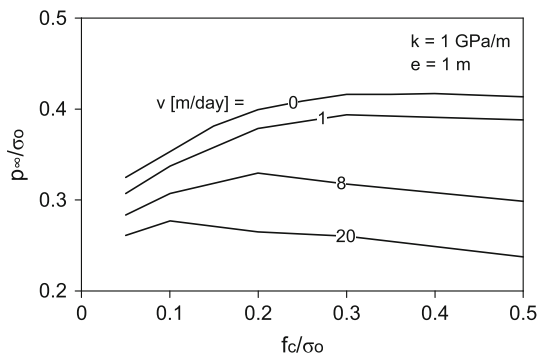**Fig. 17** Development of the ground pressure acting upon the lining for advance rates v of 0–20 m/day

Fig. 18 Normalized final lining load p_∞/σ_0 as a function of the normalized uniaxial compressive strength f_c/σ_0 and of the advance rate v

and for a higher uniaxial compressive strength f_c of the ground, while Fig. 18 provides a more complete picture of these effects on the final lining load. The results agree with those of Graziani et al. (2005) concerning the effect of the advance rate on the final lining pressure. As a consequence of the reduced stiffness of the shotcrete near the face, the counter-intuitive behaviour becomes less and less

pronounced as the advance rate increase, but nevertheless does not disappear even at very high advance rates (20 m/day). Advance rates such as this cannot be realized in combination with shotcrete.

In conclusion, the counter-intuitive model behaviour persists even when taking into account the changes to the shotcrete over time.

8 Effect of the Overcut in Shield Tunnelling

8.1 Computational Model

We shall next investigate whether the deformations that inevitably occur in shield tunnelling are such that the paradox disappears. The computations concern the same axially symmetric computational model as in Fig. 4a. The only difference is the boundary condition at the tunnel wall, which in the present case accounts, (i), for the gap existing around the shield due to the overcut ΔR (Fig. 9b) and, (ii), for the complete radial unloading of the excavation boundary at the installation point of the segmental
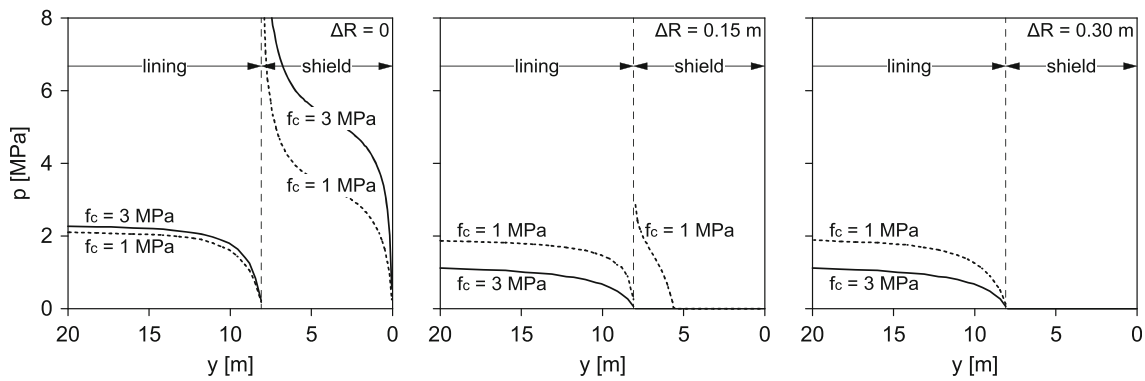
Fig. 19 Development of the ground pressure p along the tunnel (shield and lining) for two values of the uniaxial compressive strength f_c and for an overcut ΔR of 0–0.30 m

lining immediately behind the shield tail (at $y = 8$ m). Details concerning the modelling of the ground-support interface can be found in Ramoni and Anagnostou (2010a). Taking into account the modulus of elasticity of the steel ($E_S = 210$ GPa) and assuming a shield thickness of $d_S = 8$ cm, the radial stiffness of the shield is taken as $k_S = 1$ GPa/m.

8.2 Model Behaviour

Figures 19a, b and c show the distribution of the ground pressure along the tunnel (shield up to $y = 8$ m, segmental lining for $y > 8$ m) for an overcut ΔR of 0, 0.15 and 0.30 m, respectively, and for two values of the uniaxial compressive strength f_c. Let us consider first the case of zero overcut. (As an overcut is always foreseen for the purpose of steering the machine, this case is rather theoretical but may occur also in practice in exceptional cases, e.g. due to packing of the gap around the shield with fines.) The model behaviour is counter-intuitive in this case (Fig. 19a), in that the higher strength ground develops a higher load than the lower strength ground. The paradox is particularly pronounced in relation to the shield loading and also applies to the lining.

In the case of an overcut ΔR of 0.15 m or higher, however, the system allows for deformations to occur behind the face and thus the paradox disappears. According to Fig. 19b, the ground closes the gap and starts to exert a load upon the shield only in the case of the lower strength value ($f_c = 1$ MPa). In the case of an even larger overcut ($\Delta R = 0.30$ m, Fig. 19c), the gap around the shield remains open even for the lower strength value.

9 Conclusions

The computational models commonly used for tunnel design predict under certain conditions (i.e. support from a

stiff lining near to the tunnel face, weak ground, high initial stress) that the load developing upon the lining increases with the strength of the ground. Such behaviour deserves to be called a paradox because it is clearly contrary to what one would expect on the basis of intuition and tunnelling experience. The reason for this counter-intuitive behaviour is the stress relief which takes place in the ground ahead of the face and which is more pronounced in the case of a low strength ground. The decisive simplifying modelling assumptions, i.e. the assumptions which cause the difference between model behaviour and actual behaviour, are related: (i), to the rheological behaviour of the ground (which is usually neglected in design computations, but is particularly important in the case of overstressed ground, limiting the extent of stress relief ahead of the face); and, (ii), to the stiffness of the support system, which may—due to the nature of construction procedures—be considerably lower than it is assumed to be in the design calculations. The effects of face reinforcement or of the time-dependency of the shotcrete stiffness are of secondary importance with respect to the investigated aspect of the model behaviour.

The findings of the present paper illustrate the uncertainties (both quantitative and qualitative) that exist in all computational models—even in the very familiar and well-established ones—and emphasize the importance of a careful interpretation of the computational results and of a critical review of the underlying modelling assumptions. Taking into account the two main effects mentioned above in the design computations eliminates the paradoxical model behaviour.

Appendix A: Demonstration of the Meaning of the Viscosity η

In order to demonstrate the meaning of the viscosity values we examine the classic rotationally symmetric tunnel

problem under plane strain conditions. The constitutive model was presented in Sect. 4, while the model parameters are given in Table 1.

Starting from the initial state, we first simulate tunnel excavation on the assumption that it occurs instantaneously. We then carry out a transient analysis until a steady state is reached. Figure 20 shows the typical time-development of the convergence. One can see the instantaneous, excavation-induced convergence, which, as explained in Sect. 4, is purely elastic. As a measure of how rapidly the ground responds to tunnel excavation, an arbitrary characteristic time period may be adopted—for example, the time $t_{95\%}$ that must elapse in order that the time-dependent convergence reaches 95% of its final value. In the example of Fig. 20 (viscosity $\eta = 10^5$ kPa day), this time period will be about 15 days long. For dimensional reasons, the characteristic time is proportional to the viscosity η (a viscosity 10 times higher will mean that the time taken to reach a given deformation will increase by a factor of 10).

Table 2 is based upon the results of a parametric study into the effects of the uniaxial compressive strength f_c and the viscosity η on the characteristic time $t_{95\%}$ (Fig. 21).
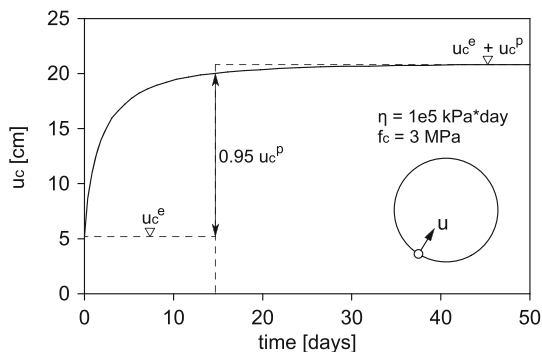

Fig. 20 Time-development of the convergence of an unsupported circular tunnel under plane strain conditions
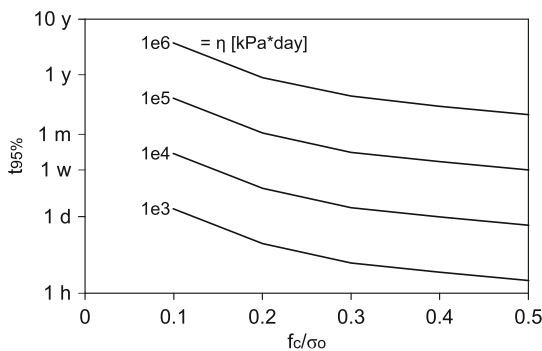

Fig. 21 Characteristic time $t_{95\%}$ as a function of the normalized uniaxial compressive strength f_c/σ_0 and of the viscosity η (the time axis labels *y*, *m*, *w*, *d* and *h* denote year, month, week, day and hour, respectively)

Appendix B: Numerical Modelling of Time-Dependent Support Stiffness

Boundary Condition for a Lining of Constant Stiffness

The resistance of a lining with constant stiffness k is taken into account in the steady state numerical solution method by imposing (as a boundary condition) a radial pressure $p(y)$ which is proportional to the deformation *of the lining* at location y and depends therefore not only on the convergence $u(y)$ of the ground but also on its deformation $u(e)$ at the installation point ($y = e$) of the lining (Anagnostou 2007):

$$p(y) = k\left(u(y) - u(e)\right). \tag{6}$$

Boundary Condition for a Lining of Time-Dependent Stiffness

In the case of a lining with time-dependent properties, however, the calculation of the pressure along the lining has to be carried out by numerical integration in the opposite direction to that of the tunnel advance (Anagnostou 2007). Figure 22a shows schematically the integration points and intervals. The pressure p_{j+1} at point $j + 1$ can be expressed by following equation:

$$p_{j+1} = p_j + \Delta p_{j+1}, \tag{7}$$

where Δp_{j+1} denotes the increase in pressure over the integration interval $j + 1$, which extends from point j to point $j + 1$:

$$\Delta p_{j+1} = k_{j+1}\left(u_{j+1} - u_j\right), \tag{8}$$

where $u_{j+1} - u_j$ is the increase in ground deformation from point j to point $j + 1$, while k_{j+1} denotes the average stiffness over the integration interval $j + 1$:
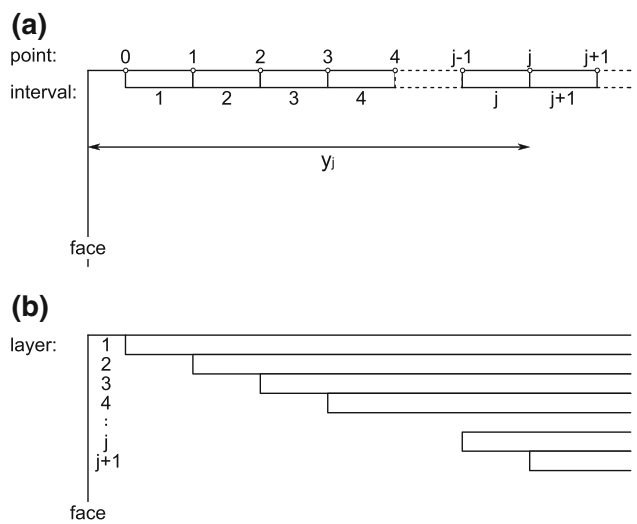

Fig. 22 **a** Definition of the lining segments and nodes, **b** Definition of the lining layers

$$k_{j+1} = \frac{E_{\mathrm{L}}(t)\,d}{a^2}, \tag{9}$$

where d is the thickness of the lining, a is the tunnel radius, $E_{\mathrm{L}}(t)$ is the Young's modulus of the lining (according to Eq. 5) and t is the age of the shotcrete. The latter depends on the distance from the face and on the advance rate:

$$t = \frac{(y_j + y_{j+1})/2}{v}. \tag{10}$$

Implementation of the Boundary Condition in the Numerical Model

The boundary condition described by the Eqs. 6–10 is implemented in the numerical model by a series of super-imposed fictitious lining layers, each having a different stiffness $k^{(i)}$ and starting at a different distance behind the face (Fig. 22b): The fictitious lining layer i starts at integration point $i-1$ (and, therefore, the radial displacement u_{i-1} represents the pre-deformation to be considered for this layer), contains all integration intervals $\geq i$ and has a stiffness which is equal to the increase in stiffness from the integration interval $i-1$ (i.e. the integration interval just before the starting point of the fictitious layer i) to integration interval i (i.e. the first integration interval belonging to fictitious layer i):

$$k^{(i)} = k_i - k_{i-1} \quad (\text{with } k_0 = 0). \tag{11}$$

It will subsequently be demonstrated that the superimposed fictitious lining layers defined in this way are equivalent to a lining with a time-dependent stiffness, i.e. they provide a total support pressure which is equal to that of Eqs. 6 and 7.

Proof

First of all, one can readily verify that Eq. 11 ensures that the total stiffness offered by the superimposed fictitious lining layers in an arbitrary interval m is equal to the stiffness k_m of the shotcrete lining over this interval. The total stiffness offered by the superimposed fictitious layers is equal to the sum of the stiffnesses of the layers containing the interval m, i.e. of the layers 1 to m. Consequently, the total stiffness is equal to

$$\sum_{i=1}^{m} k^{(i)} = \sum_{i=1}^{m} (k_i - k_{i-1}) = k_m. \tag{12}$$

As each fictitious lining layer has a constant stiffness, its resistance to deformation can be calculated on the basis of Eq. 6. Taking into account the layer stiffness according to Eq. 11, as well as the relevant pre-deformation of each layer (which as said above is equal to u_{i-1} for layer i), the

pressure exerted by an arbitrary layer i at an arbitrary point j reads as follows:

$$p_j^{(i)} = k^{(i)} \left(u_j - u_{i-1} \right) = \left(k_i - k_{i-1} \right) \left(u_j - u_{i-1} \right). \tag{13}$$

The total pressure at point m is obtained by a summation of the pressures of the layers that contain point m, i.e. of the layers 1 to m:

$$p_m = \sum_{i=1}^{m} p_m^{(i)} = \sum_{i=1}^{m} (k_i - k_{i-1}) (u_m - u_{i-1}). \tag{14}$$

Analogously, for point $m+1$,

$$\begin{aligned}
p_{m+1} &= \sum_{i=1}^{m+1} (k_i - k_{i-1}) (u_{m+1} - u_{i-1}) \\
&= \sum_{i=1}^{m} (k_i - k_{i-1}) (u_m - u_{i-1}) \\
&\quad + \sum_{i=1}^{m} (k_i - k_{i-1}) (u_{m+1} - u_m) \\
&\quad + (k_{m+1} - k_m) (u_{m+1} - u_m) \\
&= p_m + \sum_{i=1}^{m+1} (k_i - k_{i-1})(u_{m+1} - u_m) \\
&= p_m + k_{m+1}(u_{m+1} - u_m),
\end{aligned} \tag{15}$$

which agrees with Eqs. 7 and 8.

References

AFTES (2002) Recommandations relatives à la methode convergence-confinement. Association Française des Travaux en Souterrain, Groupe de travail n°7 (animé par M. Panet avec la collaboration de A. Bouvard, Dardard B, Dubois P, Givet O, Guilloux A, Launay J, Nguyen Minh Duc, Piraud J, Tournery H, Wong H). Tunnels et Ouvrages Souterrains 170:79–89

Anagnostou G (2007) Continuous tunnel excavation in a poroelastoplastic medium. In: Pande GN, Pietruszczak S (eds) Numerical models in geomechanics (NUMOG X), Rhodes, Greece, Taylor & Francis, pp 183–188

Anagnostou G, Kovári K (1993) Significant parameters in elastoplastic analysis of underground openings. J Geotech Eng 119(3):401–418

Barla G, Bonini M, Debernardi D (2008) Time dependent deformations in squeezing tunnels. In: The 12th international conference of International Association for Computer Methods and Advances in Geomechanics (IACMAG), Goa, India, pp 4265–4275

Bernaud D (1991) Tunnels profonds dans les milieux viscoplastiques: approches expérimentale et numérique. PhD Thesis, Ecole Nationale des Ponts et Chaussées, Paris, France

Boldini D, Graziani A, Ribacchi R (2000) L'analisi tensio-deformativa al fronte di scavo e nella zona del retrofronte. In: Lo scavo meccanizzato delle gallerie, mir2000-VIII ciclo di conferenze di meccanica e ingegneria delle rocce, Torino, Pàtron Editore Bologna, pp 159–216

Boldini D, Lackner R, Mang HA (2005) Ground-shotcrete interaction of NATM tunnels with high overburden. J Geotech Geoenviron Eng 131(7):886–897

Brinkgreve RBJ (2002) PLAXIS 2D, version 8. Lisse, Netherlands

Cantieni L, Anagnostou G (2009a) The effect of the stress path on squeezing behaviour in tunnelling. Rock Mech Rock Eng 42(2):289–318. doi:10.1007/s00603-008-0018-9

Cantieni L, Anagnostou G (2009b) The interaction between yielding supports and squeezing ground. Tunn Undergr Space Technol 24(3):309–322. doi:10.1016/j.tust.2008.10.001

Chang Y (1994) Tunnel support with shotcrete in weak rock—a rock mechanics study. Ph.D., Royal Institute of Technology, Stockholm, Sweden

Chern JC, Shiao FY, Yu CW (1998) An empirical safety criterion for tunnel construction. In: Regional symposium on sedimentary rock engineering, Taipei, Taiwan, pp 222–227

Debernardi D, Barla G (2009) New viscoplastic model for design analysis of tunnels in squeezing conditions. Rock Mech Rock Eng 2009(42):259–288. doi:10.1007/s00603-009-0174-6

Ehrbar H, Pfenninger I (1999) Umsetzung der Geologie in technische Massnahmen im Tavetscher Zwischenmassiv Nord. In: Vorerkundung und Prognose der Basistunnels am Gotthard und am Lötschberg, Symposium Geologie Alptransit, Zurich, Switzerland, A.A.Balkema Rotterdam Brookfield, pp 381–394

Gioda G, Cividini A (1996) Numerical methods for the analysis of tunnel performance in squeezing rocks. Rock Mech Rock Eng 29(4):171–193

Graziani A, Boldini D, Ribacchi R (2005) Practical estimate of deformations and stress relief factors for deep tunnels supported by shotcrete. Rock Mech Rock Eng 38(5):345–372

Guo C (1995) Calcul des tunnels profonds soutenus - méthode stationnaire et méthodes approchées. PhD Thesis, Ecole Nationale des Ponts et Chaussées, Paris, France

Itasca (2006) Flac2D 5.0, User's Manual. Itasca Inc., Minneapolis, USA

Kasper T, Meschke G (2006) On the influence of face pressure, grouting pressure and TBM design in soft ground tunnelling. Tunn Undergr Space Technol 21(2):160–171

Kovári K, Staus J (1996) Tunnelbau in druckhaftem Gebirge, Falldarstellungen. ETH Zurich, Institut für Geotechnik, August 1996

Lavdas N (2010) Einsatzgrenzen von Tübbingausbau beim TBM - Vortrieb in druckhaftem Gebirge. Master Thesis, ETH Zurich, Zurich, Switzerland

Lunardi P (2000) The design and construction of tunnels using the approach based on the analysis of controlled deformation in rocks and solis. Tunnels & Tunnelling International special supplement, ADECO-RS approach (May)

Madejski J (1960) Theory of non-stationary plasticity explained on the example of thick-walled spherical reservoir loaded with internal pressure. Archiwum Mechaniki Stosowanej 5/6(12):775–787

Mair RJ (2008) Tunnelling and geotechnics: new horizons. Géotechnique 58(9):695–736. doi:10.1680/geot.2008.58.9.695

Nguyen-Minh D, Corbetta F (1991) New calculation methods for lined tunnels including the effect of the front face. In: 7th Congress of the ISRM, Aachen, pp 1334–1338

Nguyen-Minh D, Corbetta F (1992) New methods for rock-support analysis of tunnels in elastoplastic media. In: McCreath K (ed) Rock support in mining and underground construction, Sudbury, Canada, Balkema, Rotterdam, pp 83–90

Nguyen-Minh D, Guo C (1993) Sur un principe d' interaction massif-soutenement des tunnels en avancement stationnaire. In: Ribeiro Sousa L, Grossmann NF (eds) Eurock'93, Lisboa, Portugal, Balkema, Rotterdam, pp 171–177

Nguyen-Minh D, Guo C (1996) Recent progress in convergence confinement method. In: Barla G (ed) Eurock'96, Torino, Italy, Balkema, pp 855–860

Oreste PP (2003) A procedure for determining the reaction curve of shotcrete lining considering transient conditions. Rock Mech Rock Eng 36(3):209–236

Oreste P, Peila D, Pelizza S (2004) Face reinforcement in deep tunnels. Felsbau 22(4):20–25

Panet M (1995) Le calcul des tunnels par la méthode convergence-confinement. Presses de l'école nationale des ponts et chaussées, Paris, France

Peila D (1994) A theoretical study of reinforcement influence on the stability of a tunnel face. Geotech Geol Eng 12:145–168

Perzyna P (1966) Fundamental problems in viscoplasticity. Adv Appl Mech 9:243–377

Pöttler R (1990) Time-dependent rock–shotcrete interaction. A numerical shortcut. Comput Geotech 9:149–169

Ramoni M, Anagnostou G (2010a) The interaction between shield, ground and tunnel support in TBM tunnelling through squeezing ground. Rock Mech Rock Eng. doi:101007/s00603-010-0103-8 (available online)

Ramoni M, Anagnostou G (2010b) Thrust force requirements for TBMs in squeezing ground. Tunn Undergr Space Technol 25(4):433–455

Vlachopoulos N, Diederichs MS (2009) Improved longitudinal displacement profiles for convergence confinement analysis of deep tunnels. Rock Mech Rock Eng 42:131–146

Wong H, Trompille V, Dias D (2004) Extrusion analysis of a bolt-reinforced tunnel face with finite ground-bold bond strength. Can Geotech J 41:326–341. doi:10.1139/T03-084